Electronic Supplementary Material (ESI) for RSC Advances.

Electronic Supplementary Information

Poly(vinylidenefluoride) polymers and copolymers as versatile hosts for luminescent solar concentrators: compositional tuning for enhanced performance

*Francesca Corsini,[a] Marco Apostolo,[b] Chiara Botta,[c] Stefano Turri,[a] Gianmarco Griffini[a]**

[a]Department of Chemistry, Materials and Chemical Engineering "Giulio Natta", Politecnico di Milano, Piazza Leonardo da Vinci 32, 20133 Milano,Italy.

[b]Solvay Specialty Polymers, Viale Lombardia, 20, 20021 Bollate, Italy.

[c]Institute of Sciences and Chemical Technologies "Giulio Natta" (SCITEC) of CNR, via Corti 12, 20133 Milano, Italy

*Corresponding author: gianmarco.griffini@polimi.it

Table of contents

S1. Differential scanning calorimetry (DSC) of the pure fluoropolymer

The glass transition temperatures (T_g) of the pure fluorinated polymers considered in this work are reported in Figure S1. T_g was found to increase from -40°C for homopolymer to -14°C for terpolymer due to the decreasing mobility of the amorphous phase.

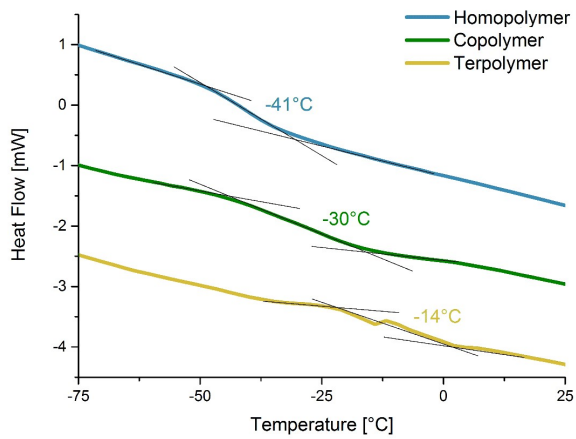

Figure S1. A detail of the DSC curves of curves of PVDF homopolymer, copolymer and terpolymer indicating the glass transition temperature.

The melting peaks, and the relative melting temperatures (T_{melt}) of the pure fluorinated polymers considered in this work are reported in Figure S2. The value of the melting temperature resulted to decrease passing from pure homopolymer to copolymer and terpolymer because of the presence of chlorotrifluoroethylene (CTFE) and hexafluoropropylene-co-hydroxylethylacetate (HFP/HEA) respectively, that cause a reduction of both melting point and degree of crystallinity.

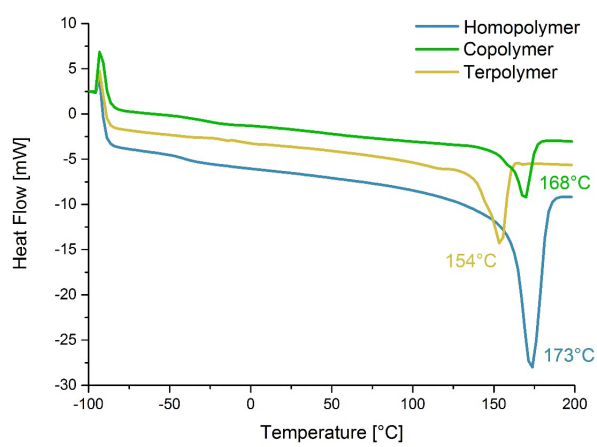

Figure S2. DSC curves of PVDF homopolymer, copolymer and terpolymer. Melting temperatures of corresponding polymer are indicated.

S2. Differential scanning calorimetry (DSC) of the fluoropolymer/PMMA blend coatings

DSC analysis was also used to evaluate the compositional effect of fluoropolymer/PMMA blend on the glass transition temperature, melting temperature and degree of crystallinity (X_C). Fluoropolymer/PMMA blends were expected to display an increase in T_g due to the higher T_g of PMMA (~100°C) accompanied by a reduction of the melting temperature and degree of crystallinity that is accentuated with the decrease in fluoropolymer/PMMA ratio.

The degree of crystallinity reduces from 49% for pure homopolymer to 26% for terpolymer and 17% for copolymer samples. Moreover, as can be observed in Figure S3, the presence of PMMA results in a further reduction in crystallinity in each fluoropolymer/PMMA blend, until a complete amorphous structure is obtained in terpolymer and copolymer blends with a PMMA content higher than 40% and 50% respectively. It can be assumed, therefore, that the presence of PMMA progressively suppresses PVDF crystallinity.

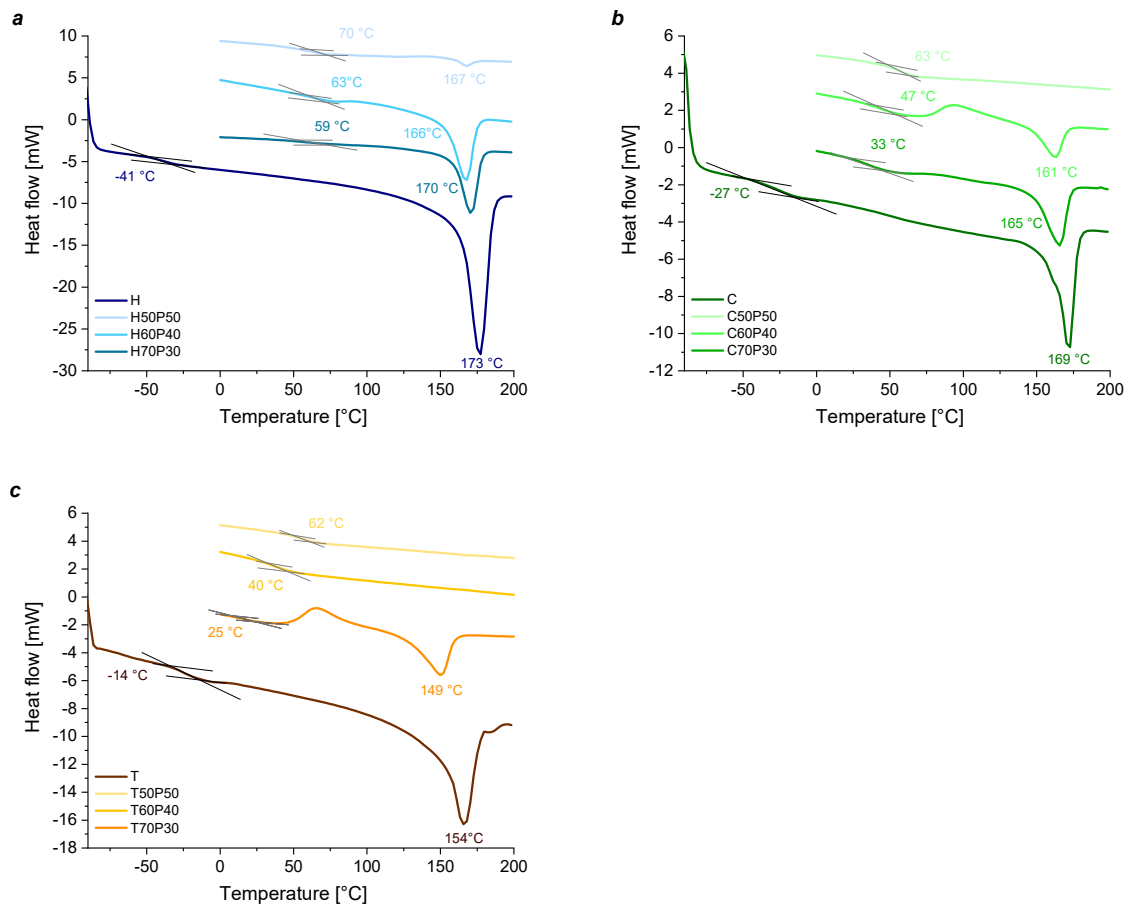

Figure S3. DSC curves of pure (a) homopolymer, (b) copolymer and (c) terpolymer and their corresponding blends with PMMA at different fluoropolymer/PMMA ratios.

S3. Scanning electron microscopy

In order to investigate the surface morphology of fluoropolymer-based systems scanning electron microscopy (SEM) was used. For this purpose, copolymer-PMMA blends were considered, as this system was found to be the most promising in terms of degree of crystallinity. Samples were prepared according to a procedure described in the literature.[S1-S3] In brief, self-standing films of copolymer/PMMA were dipped in glacial acetic acid in order to selectively remove the PMMA phase, allowed to dry and finally gold sputtered in vacuum prior to observation.

At high magnifications (10000X and 50000X), the presence of cavities due to selective etching of PMMA can be observed as shown in Figure S4 and Figure S5, respsectively. Their size grows when the PMMA content increases, as can be reasonably expected.

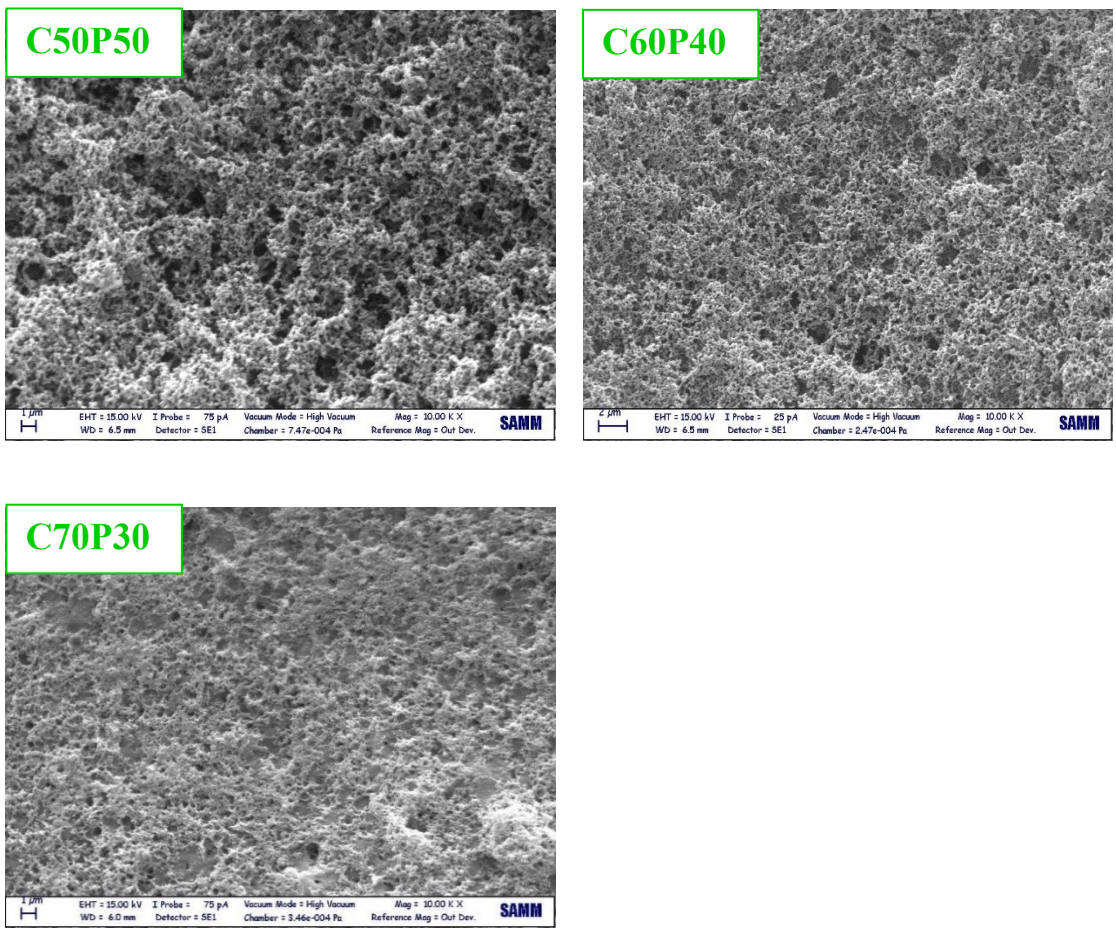

Figure S4. Surface SEM micrographs of copolymer/PMMA blends at 10000X magnification.

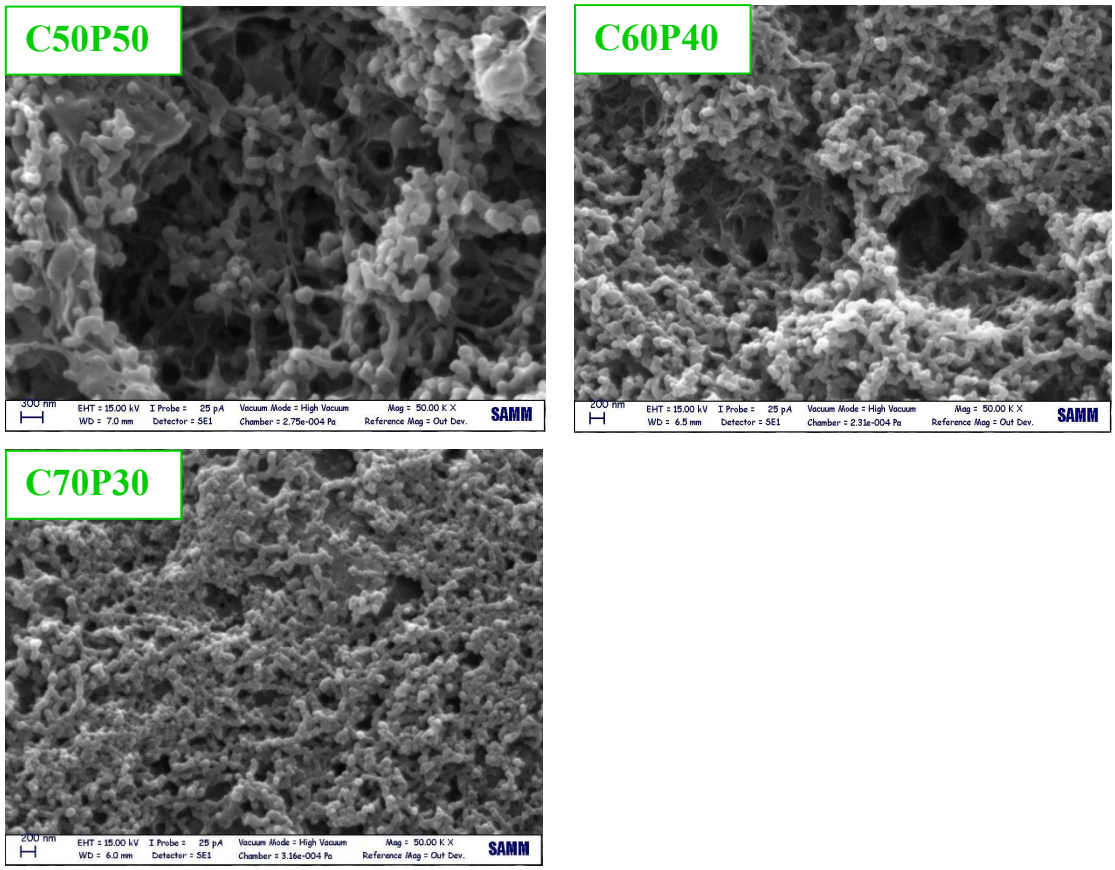

Figure S5. Surface SEM micrographs of Copolymer-PMMA blends at 50000X magnification.

S4. X-ray diffraction (XRD) analysis

The crystallinity of all polymer systems was further investigated by means of X-ray diffraction measurements (Figure S6). Spin coated samples of pure homopolymer, copolymer and terpolymer were prepared along with their corresponding fluoropolymer-PMMA blends with different PMMA/fluoropolymer ratio. Pure homopolymer samples showed different peaks at 17.8°, 18.3°, 19.9° and 26.7° indicating the presence of non-polar PVDF α phase, the most stable and common PVDF crystalline phase at ambient temperature and pressure.

The intensity of all crystallinity peaks decreases as the PMMA content increases from zero to 50% wt. indicating a progressively suppression of PVDF crystallinity. The formation of a broad band between 10° and 20° is related to the presence of amorphous phase in PMMA. Similar considerations can be done on XRD patterns of copolymer and terpolymer-based blends, where an analogous decrease in peak intensity was observed at increasing PMMA content in the blend. The presence of the fluorescent organic dye in the systems did not affect the observed trends.

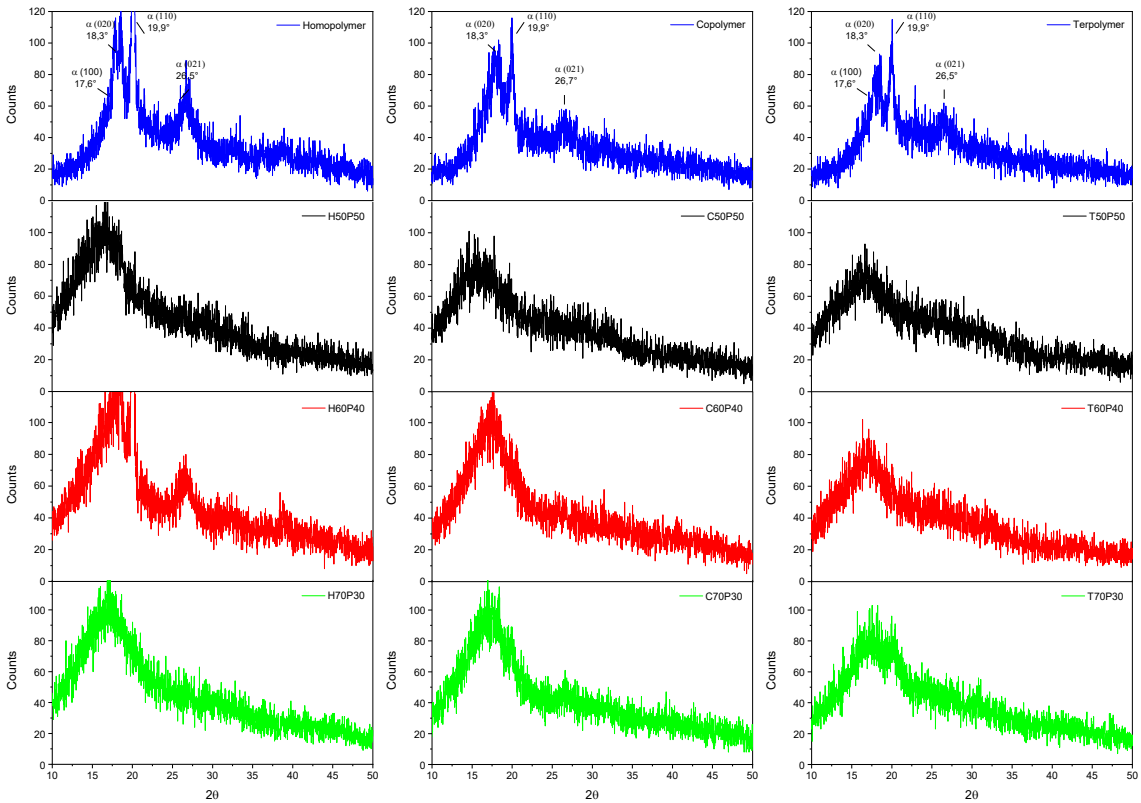

Figure S6. X-Ray diffraction curves of the systems investigated in this work.

S5. Fourier-transform infrared (FTIR) spectroscopy

The effect of the presence of the amorphous phase in PMMA on the molecular characteristics of the resulting fluoropolymer/PMMA blends was also examined by means of FTIR spectroscopy. FTIR assignments of characteristic groups of PVDF and PMMA are reported in Table S1.

Table S1. PVDF and PMMA characteristic FTIR peaks with corresponding vibrational modes.

SAMPLE	Wavenumbers [cm^{-1}]	Phase	Assignment	Reference
PMMA	2995	-	CH_3 stretching	S4
	2951	-	C-O-CH_3 stretching	S3
	1728	-	acrylate carboxyl group stretching	S4
	1485	-	CH_2 asymmetrical bending	S1
	1448	-	CH_3-O asymmetrical stretching	S1, S4, S5
	1387	-	α-methyl group	S4
	1273	-	COC stretching	S4
	1242	-	CO stretching	S1, S4
	1194	-	Skeletal chain	S1, S4
	1149	-	COC stretching	S4
	1065	-	characteristic absorption vibration	S4
	989	-	CH_3-O bending	S1, S4
	841	-	characteristic absorption vibration	S4
	754	-	CH_3 wagging deformation	S1, S4
PVDF	1423	-	CH_2 bending	S6
	1402	-	CH_2 stretching	S2, S7
	1382	α	CH_2 bending CH_2 wagging	S6
	1278	-	CF_2 symmetrical stretching	S2
	1211	α	CF_2 symmetrical stretching	S6
	1182	-	CF_2 symmetrical stretching	S5
	1149	-	CC asymmetrical stretching	S6
	1070	α	S1	S1
	975	α	CH_2 twisting	S2, S6
	872	α	CC symmetrical stretching	S3
	854	α	CH_2 rocking	S2, S6
	795	α	CH_2 rocking	S2, S6
	764	α	In plane bending or rocking	S2, S5
	615	α	CF_2 bending CCC skeletal vibrations	S2, S6

FTIR spectra of pure homopolymer compared with its PMMA blends, reported in the main text, demonstrate the progressive reduction of X_C in the blend-based coatings with the increase in PMMA mass content.

Relevant FTIR spectra of C- and T-based coating systems, reported in Figure S7, confirm that the mechanism for crystallization suppression is analogous in all three blend combinations explored in this work.

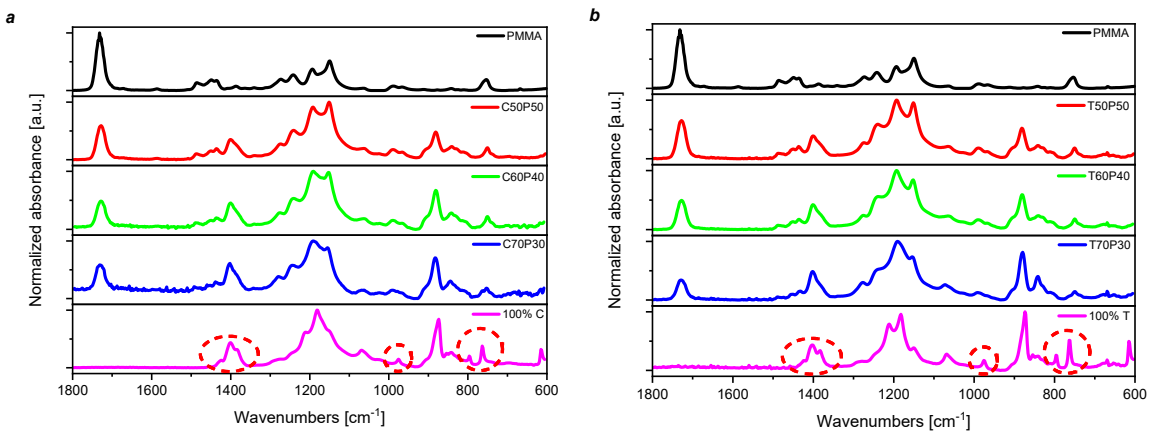

Figure S7. FTIR spectra of (a) pure copolymer compared with its PMMA blends and (b) pure terpolymer compared with its PMMA blends. Red circles indicate some characteristic PVDF groups disappearing when PMMA content is increased.

S6. Fluoropolymer/PMMA blends as host matrices: optical characterization

UV-visible absorption and fluorescence spectroscopic analyses were performed on C50P50Lz, H50P50Lz, T50P50Lz systems as a function LR305 concentration with respect to PMMA content, to determine the optimal luminophore concentration.

As can be noticed in Figure S8, for all considered fluoropolymer types the emission maximum was achieved for 5 wt.% LR305 concentration with respect to PMMA content.

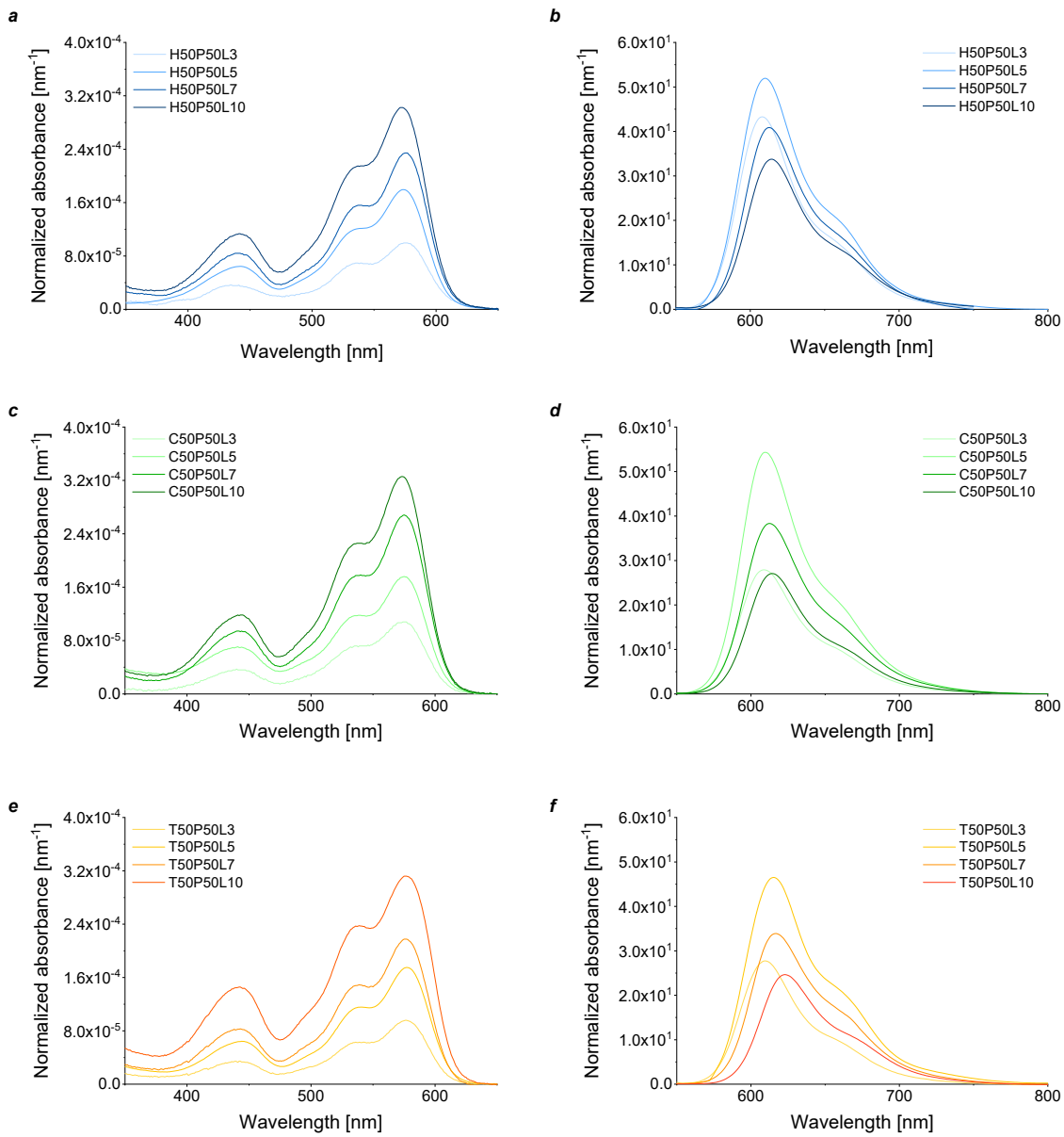

Figure S8. UV-visible absorption and fluorescence emission spectra of LR305-doped fluoropolymer blends with PMMA fixed at 50% fluoropolymer weight content as a function of the fluorophore content (from 3 to 10 wt. %) for (a,b) homopolymer, (c,d) copolymer and (e,f) terpolymer.

In addition, UV-visible absorption spectroscopy was employed on blend-based samples with different fluoropolymer to PMMA ratio in order to study the optical response of these systems and to verify any influence of the blend composition on the optical properties themselves. To this end, LR305 concentration with respect to PMMA content was maintained constant and equal to the optimal concentration (5% wt).

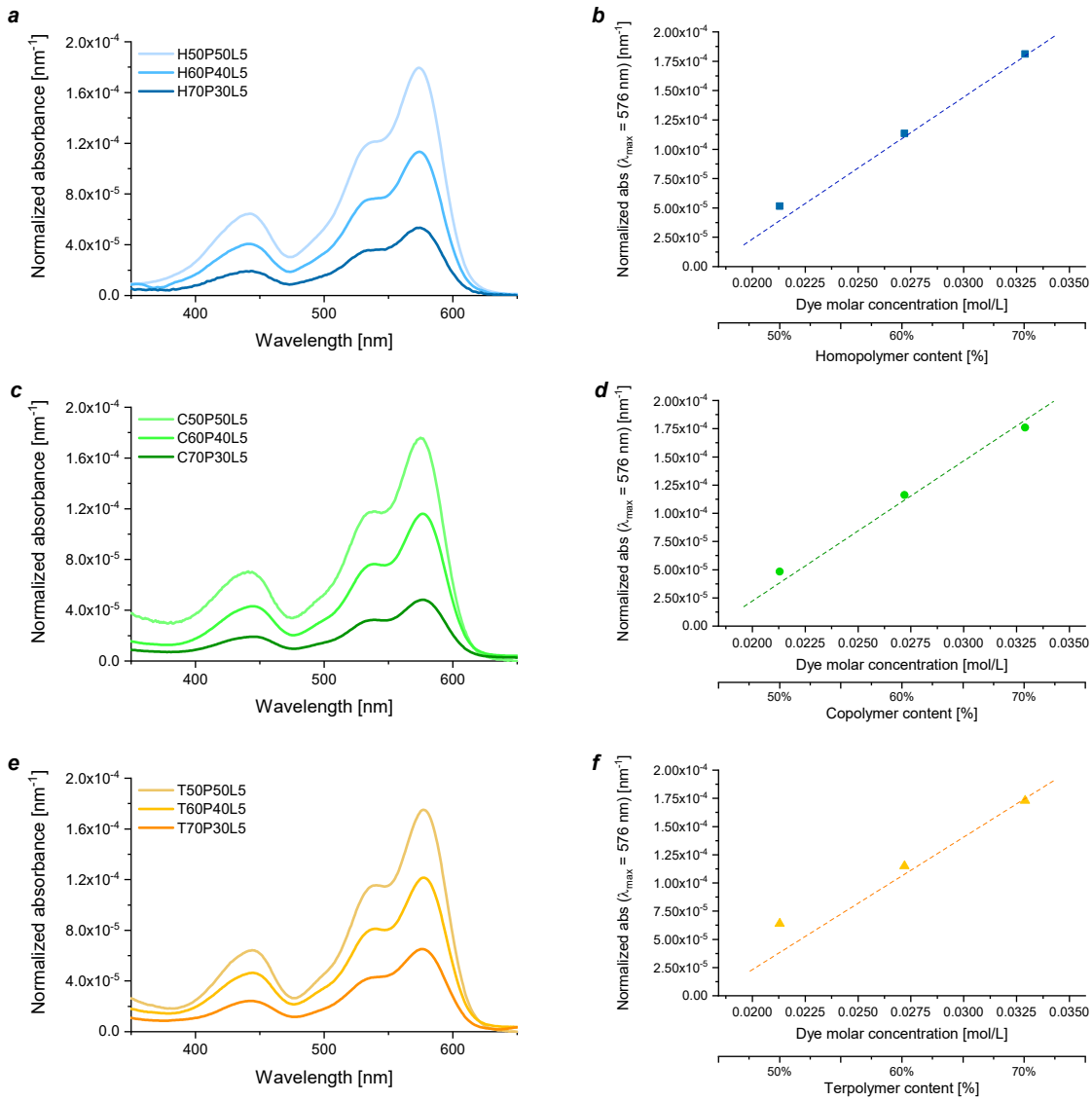

Figure S9. (a,c,e) UV-Vis absorption spectra divided by respective sample thickness in 350-650 nm region of fluoropolymer matrices at different fluoropolymer content, namely 50%, 60% and 70%. (b,d,f) Plot of absorbance main peak (576nm) *vs.* dye molar concentration for fluoropolymer-based systems.

As Figure S9 shows, display the UV-Vis absorption spectra in the 350-650 nm region for copolymer-based samples at no dependence of the optical properties on the blend composition were observed in all considered systems (H, C, T).

The fluorescence emission spectra of dye-doped fluoropolymer (H, C, T) blends with PMMA at 50, 60 and

70% fluoropolymer weight content and fixed dye content (5 wt. %) are reported in Figures S10a-c. At every fluoropolymer/PMMA ratio, the fluorescence process appears to be more efficient in copolymer-based systems, likely due to a different degree of crystallinity with respect to H and T-based systems.

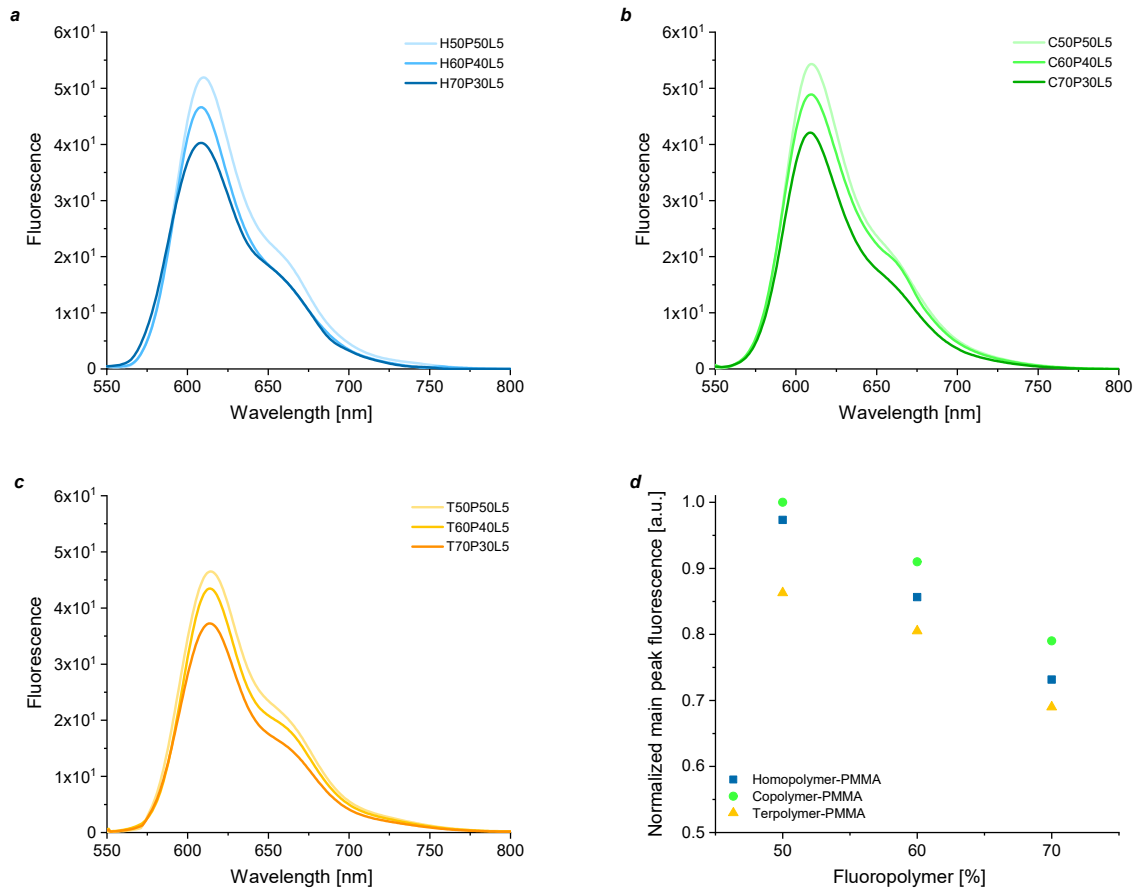

Figure S10. Fluorescence emission spectra of dye-doped fluoropolymer blends with PMMA at 50, 60 and 70% fluoropolymer weight content and fixed dye content (5 wt. %) for (a) homopolymer, (b) copolymer and (c) terpolymer. The excitation wavelength is λ_{exc} = 445 nm. (d) Normalized fluorescence intensity at the main emission peak (605 nm) of dye doped fluoropolymer/PMMA blend matrices at different fluoropolymer content, namely 50%, 60% and 70%

S7. Fluoropolymer/PMMA blends-based LSCs: device characterization

The investigation of the effect of the main LSC device parameters (dye concentration, polymer matrix to solvent ratio, blend composition and LSC thin film thickness) on performance was carried out on both LSCs and LSC-PV assemblies through photonic and photovoltaic characterization.

The external and internal photon efficiency (η_{ext}, η_{int}) of the LSC as a photonic device are defined as follows:[S8]

$$\eta_{int} = \frac{N_{ph-out}}{N_{ph-abs}} = \frac{\sum_{i=1}^{4} \int_{300}^{800} P_{i(out)}(\lambda) \frac{\lambda}{hc} d\lambda}{\int_{300}^{800} P_{in}(\lambda) \frac{\lambda}{hc} (1 - 10^{-A(\lambda)}) d\lambda} \quad (S1)$$

$$\eta_{ext} = \frac{N_{ph-out}}{N_{ph-in}} = \frac{\sum_{i=1}^{4} \int_{300}^{800} P_{i(out)}(\lambda) \frac{\lambda}{hc} d\lambda}{\int_{300}^{800} P_{in}(\lambda) \frac{\lambda}{hc} d\lambda} \quad (S2)$$

where λ, h and c are the wavelength of light (in nm), the Planck's constant (in J s) and the speed of light (in m s^{-1}), respectively. $P_{i(out)}(\lambda)$ is the output power spectrum measured for each edge of the LSC (in W nm^{-1}), and $P_{in}(\lambda)$ is the input power spectrum from the solar simulator incident on the top surface of the LSC (in W nm^{-1}) and $A(\lambda)$ is the absorption spectrum of the LSC. The integrations of the incident and output power spectra were performed in the 300-800 nm range of the AM1.5G solar spectrum.
For the evaluation of η_{ext}, the output of the solar simulator was calibrated to 1 Sun (100 ± 10 mW cm^{-2}). The solar simulator produced an illumination spot that covered the entire surface area of the LSC device, which was placed on an absorbing black background to avoid photon double pass effects.

The optical photovoltaic efficiency (η_{LSC-PV}) of the LSC-PV assembly was defined as:

$$\eta_{LSC-PV} = \frac{\eta_{PCE,LSC}}{\eta_{PCE,PV}} = \frac{I_{sc,LSC}}{I_{sc,PV} \cdot G} \quad (S3)$$

where $I_{sc,LSC}$, $I_{sc,PV}$, and G are the short-circuit current of the LSC-PV device, of the PV cell alone and the geometric gain factor, respectively. The latter is given by the ratio of the LSC top surface area (50 x 50 mm^2) and the area of LSC four-edges ([6 x 50 mm^2] x 4).

The concentration factor *C*, namely the ratio of the incident and output photon flux density of the LSC, was also evaluated as it allows to assess the real performances provided by the LSC-PV collector. Hence, C can be defined as:

$$C = \eta_{ext} \cdot G \quad (S4)$$

where η_{ext} and G are the external photon efficiency of the LSC device and the geometric gain factor.

a. Effect of luminophore concentration

The effect of luminophore concentration on the performance of the fluoropolymer/PMMA blends-based LSC systems was first investigated. A summary of all LSC and LSC-PV devices at increasing dye concentration on the systems is reported in Figure S11 and Table S2, respectively. In every system considered η_{ext} and $\eta_{LSC\text{-}PV}$ reach a maximum value at 5 wt.% LR305 concentration. Meanwhile, η_{int} was found to be nearly constant up to the threshold concentration of 5 wt.% LR305 concentration, above which a general decrease in LSC performance was observed. This trend might be ascribed to the presence of dissipative processes such as fluorescence quenching (due to either reabsorption events or dye aggregation) which become more prominent at high doping levels.

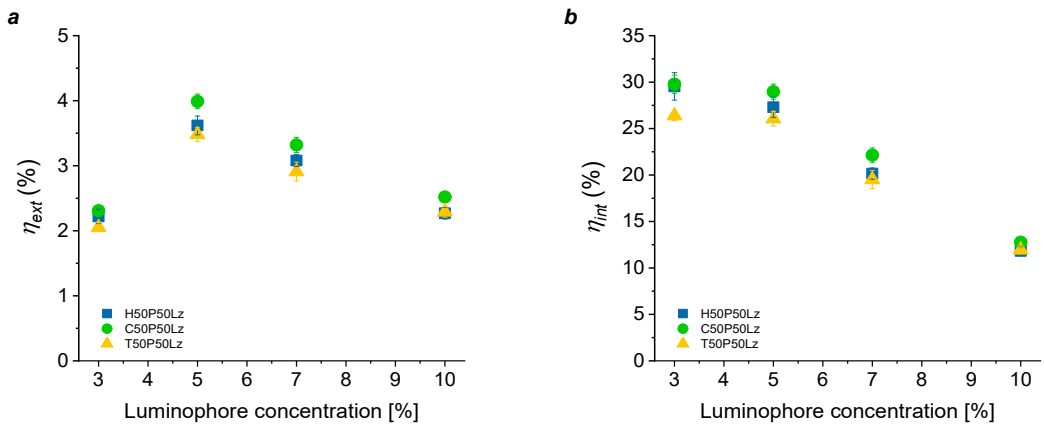

Figure S11. (a) η_{ext}, (b) η_{int} *and (C)* $\eta_{LSC\text{-}PV}$ versus LR305 content for C50P50Lz, O50P50Lz, T50P50Lz systems, z is the dye concentration with respect to PMMA content.

Table S2. Main LSC device parameters for homopolymer, copolymer and terpolymer-based systems at increasing luminophore concentration.

MATRIX	Dye content [%]	$I_{SC,LSC}$ [mA]	$V_{OC,LSC}$ [V]	FF_{LSC} [%]	$\eta_{LSC\text{-}PV}$ [%]	*C*
H50P50Lz	**3**	9.04	2.14	47.82	2.68	0.046
	5	11.29	2.18	49.50	3.54	0.076
	7	10.11	2.15	52.83	3.34	0.064
	10	8.76	2.13	51.04	2.83	0.047
C50P50Lz	**3**	9.95	2.15	49.21	3.05	0.048
	5	12.37	2.15	48.42	3.77	0.083

	7	10.92	2.14	50.50	3.44	0.069
	10	9.15	2.11	51.97	2.90	0.053
T50P50Lz	**3**	7.62	2.14	49.59	2.31	0.043
	5	10.35	2.15	50.66	3.27	0.073
	7	8.84	2.17	51.23	2.85	0.061
	10	8.03	2.16	50.48	2.54	0.048

b. Effect of coating thickness

The effect of coating thickness on the optical efficiency was examined first by changing the polymer concentration in solution at fixed deposition speed and then by varying the spin coating speed at a fixed polymer matrix to solvent ratio.
As displayed in Table S3, an increasing trend in device performance with respect to thickness can be observed.

Table S3. Main LSC device parameters for homopolymer, copolymer and terpolymer-based systems at different polymer-matrix-to-solvent ratios and spin coating speed.

MATRIX	**Thickness [μm]**	**$I_{SC,LSC}$ [mA]**	**$V_{OC,LSC}$ [V]**	**FF_{LSC} [%]**	**$\eta_{LSC\text{-}PV}$ [%]**	***C***
H50P50L5	0.951 ± 0.037	8.72	2.17	50.02	2.75	0.054
	1.604 ± 0.041	11.29	2.18	49.50	3.54	0.076
	2.978 ± 0.106	11.88	2.16	49.11	3.66	0.080
C50P50L5	0.956 ± 0.048	8.99	2.17	50.71	2.95	0.061
	1.593 ± 0.039	12.37	2.15	48.42	3.77	0.083
	3.111 ± 0.099	12.92	2.17	49.51	3.93	0.091
T50P50L5	0.949 ± 0.046	9.12	2.15	48.41	2.72	0.054
	1.597 ± 0.054	10.35	2.15	50.66	3.27	0.073
	3.052 ± 0.115	11.16	2.16	49.02	3.43	0.075

c. Effect of blend composition

The effect of PMMA content in blend composition (fluoropolymer to PMMA ratio) on device performance was also studied. In general, as the fluoropolymer content increases, the LSC performance shows a sharp decrease. From Table S4, it can be observed that copolymer blends performed better at every fluoropolymer/PMMA ratio considered and, at the same time, the terpolymer-based systems showed the lowest performance.

Table S4. Main LSC device parameters for homopolymer, copolymer and terpolymer-based systems at different fluoropolymer/PMMA ratios.

MATRIX	PVDF content [wt. %]	PMMA content [wt. %]	$I_{SC,LSC}$ [mA]	$V_{OC,LSC}$ [V]	FF_{LSC} [%]	η_{LSC-PV} [%]	C
Homopolymer	**50**	**50**	11.29	2.18	49.50	3.54	0.075
	60	**40**	9.68	2.17	50.34	3.06	0.057
	70	**30**	7.68	2.17	49.85	2.41	0.042
Copolymer	**50**	**50**	12.37	2.15	48.42	3.77	0.083
	60	**40**	9.95	2.16	51.46	3.21	0.062
	70	**30**	7.92	2.17	49.11	2.44	0.051
Terpolymer	**50**	**50**	10.35	2.15	50.66	3.27	0.073
	60	**40**	9.43	2.17	51.59	3.18	0.047
	70	**30**	7.41	2.16	48.17	2.25	0.039

Also, as Table S5 shows, PLQY measurements carried out on the three different fluoropolymer/PMMA systems at a fixed blend composition (50:50) and luminophore concentration (5 wt.%) confirmed that copolymer blend outperformed the other two proposed systems. This evidence could be ascribed to the limited homogeneity of terpolymer thin films which causes scattering phenomena. Instead, the lower performances of homopolymer-based systems with respect to pure copolymer-based counterparts is likely due to the higher amount of crystalline phase in the homopolymer as revealed from DSC analyses. These considerations led to the choice of copolymer-PMMA blends as optimal candidate to be used as LSC host matrix.

Table S5. PLQY values for H50P50L5, C50P50L5 and T50P50L5 systems

MATRIX	PLQY [%]
Homopolymer	39
Copolymer	45
Terpolymer	25

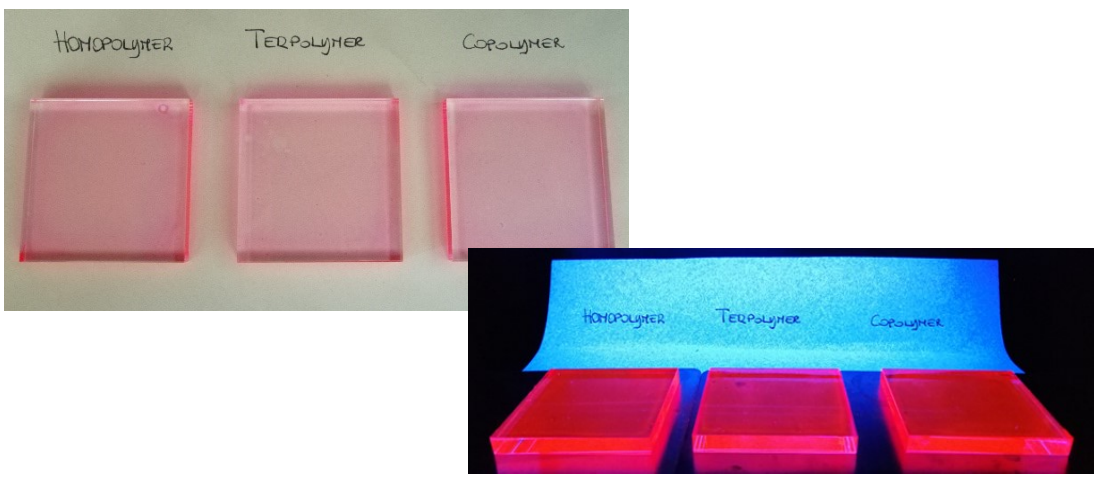

Figure S12. Photographic images of H50P50L5, C50P50L5 and T50P50L5 LSC systems both under visible and UV illumination.

S8. Fluoropolymer/PMMA blends-based LSCs: device architecture optimization

To demonstrate the factual potential of copolymer blend-based LSC devices, their performance was compared with state-of-art PMMA-based systems. The optimized copolymer/PMMA blends with different fluoropolymer content, namely 50%, 60% and 70%, and a LR305 concentration of 5 wt.% vs. total dye polymers was finally considered. Also, PMMA-based LSC counterpart (P10L5) was produced as a reference. The polymer was dissolved in chloroform at 10% solid weight content and LR305 was added at a concentration of 5% on PMMA. The film thickness for fluoropolymer-based and reference PMMA-based LSC coatings was maintained constant (~3 μm) to achieve samples with the same optical density.
The average $\eta_{LSC\text{-}PV}$ obtained for these systems is shown in Figure S13.

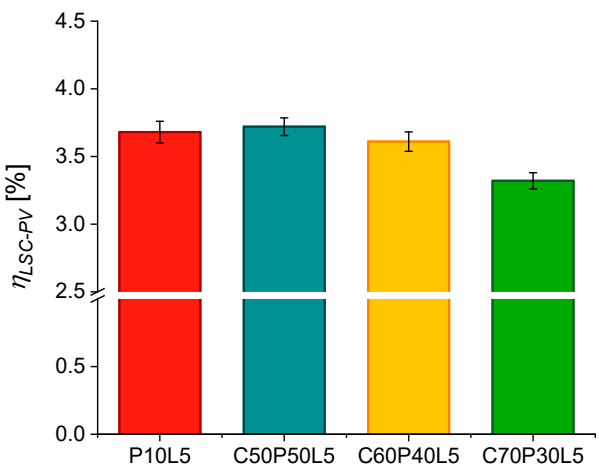

Figure S13. Average $\eta_{LSC\text{-}PV}$ of the optimized four-cell LSC devices.

As shown in the bar plot, the average $\eta_{LSC\text{-}PV}$ values of copolymer-based devices at low fluoropolymer content (50% and 60% weight concentration, C50P50L5 and C60P40L5) are comparable to the values reached by PMMA-based LSCs while high fluoropolymer content (C70P30L5) gives slightly lower performance. In conclusion, host matrix systems realized with copolymer/PMMA blends prove to be comparable in term of PV performances with respect to pure PMMA, which represents the state-of-the-art matrix in LSC devices.

S9. Fluoropolymer/PMMA blends-based LSCs: accelerated weathering tests

Accelerated weathering tests were performed to characterize the long-term durability behavior of the fluorinated/PMMA blends-based systems presented in the previous sections.
As described in detail in the Experimental section, with this aim LSC/PV-cell assemblies were placed in a weather-o-meter chamber and continuously illuminated under Xenon light. The spectrum of the source is reported in Figure S14.

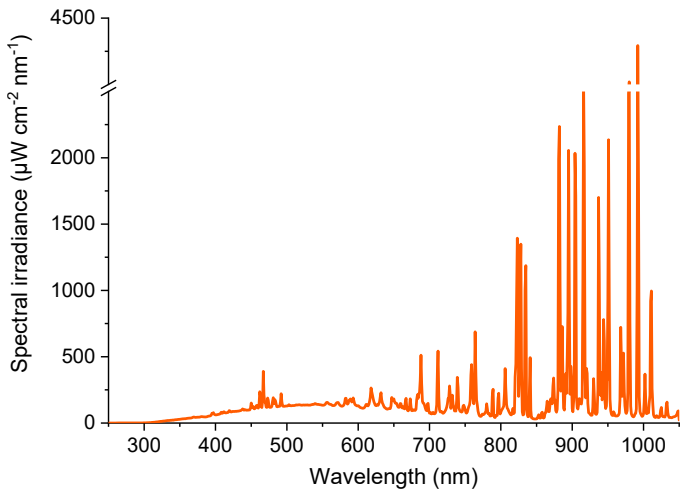

Figure S13. O-meter chamber Xenon lamp spectral irradiance as a function of wavelength.

First, the weathering behaviour of the LSC devices was studied by analysing the PV performances over time. A general decrease in output power was observed in PMMA-based samples while copolymer/PMMA blends retained their initial performance even after 1000 hours exposure. The latter results indicated that fluoropolymer-based LSC are characterized by longer photostability with respect to PMMA-based reference system. This was further confirmed by FTIR analysis outcomes.
Indeed, as Figure S15a shows, the evolution of the FTIR spectrum of PMMA-based samples was monitored at increasing light exposure time (0 h, 500 h and 1000 h). Along with the spectra in the 2000-600 cm^{-1} region, detailed zooms of FTIR spectra are also provided in the region where the characteristic peaks of the fluorescent dye can be observed. In particular, the band located at 1672 cm^{-1} is associated with the C=O stretching vibration in the organic dye molecule; the band at 1587 cm^{-1} is related to the aromatic C=C stretching vibrations of perylene core; the band at 1340 cm^{-1} is again to be assigned to vibrations of the perylene core and, at last, the band at 877 cm^{-1} can be attributed to the lateral substituents and more specifically to a phenyl ring "breathing" localized on the –O-Ph groups.[S9] In PMMA-based reference system after long-term exposure the intensity of the characteristic peaks attributed to organic dye are found to decrease indicating a possible degradation of its lateral substituents. Moreover, prolonged light exposure led to the appearance of two bands in the carbonyl region adjacent to the main C=O stretching peak that may be attributed to the formation of oxidation products in the dye molecule and in the polymeric matrix. Conversely, as depicted in Figure S15b, the overlap of FTIR spectra of fluoropolymer-based blends over 1000 hours of prolonged light exposure demonstrated no significant molecular modifications had occurred.

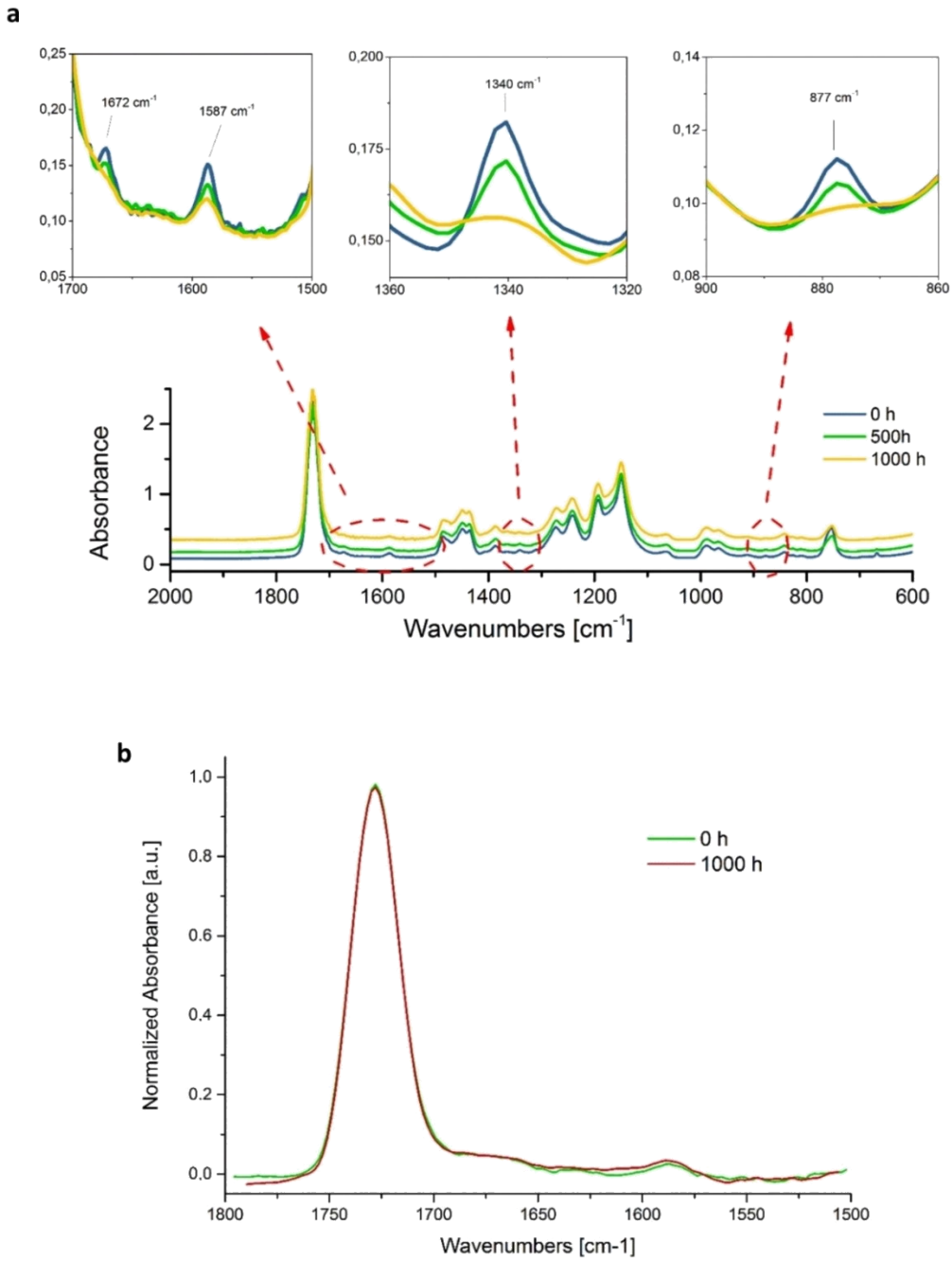

Figure 15. (a) FTIR spectra of P20L5 system after 0, 500 and 1000 hours exposure time. Some details regarding LR305 characteristic peaks are also provided. (b) Normalized FTIR spectra in the 1800-1500 cm^{-1} region of C50P50L5 system after 0 h and 1000 h exposure time under a weather-o-meter chamber.

References

S1 I.S. Elashmawi, N.A. Hakeem, *Polym. Eng. Sci.*, 2008, **48**, 895–901.

S2 M. Sharma, K. Sharma, S. Bose, *J. Phys. Chem. B*, 2013, **117**, 8589–8602.

S3 J. Cheng, J. Zhang, X. Wang, *J. Appl. Polym. Sci.*, 2013, **127**, 3997–4005.

S4 G. Duan, C. Zhang, A. Li, X. Yang, L. Lu, X. Wang, *Nanoscale Res. Lett.*, 2008, **3**, 118–122.

S5 S. Mohamadi, In *Infrared Spectroscopy - Materials Science, Engineering and Technology*; 2012; pp 213–232.

S6 M. Kobayashi, K. Tashiro, H. Tadokoro, *Macromolecules*, 1975, **8**, 158–171.

S7 S. Golcuk, A.E. Muftuoglu, S.U. Celik, A. Bozkurt, *J. Polym. Res.*, 2013, **20**, 144.

S8 M.G. Debije, R.C. Evans, G. Griffini, *Energy Environ. Sci.*, 2021, **14**, 293–301.

S9 G. Griffini, L. Brambilla, M. Levi, M. Del Zoppo, S. Turri, *Sol. Energy Mater. Sol. Cells*, 2013, **111**, 41–48.